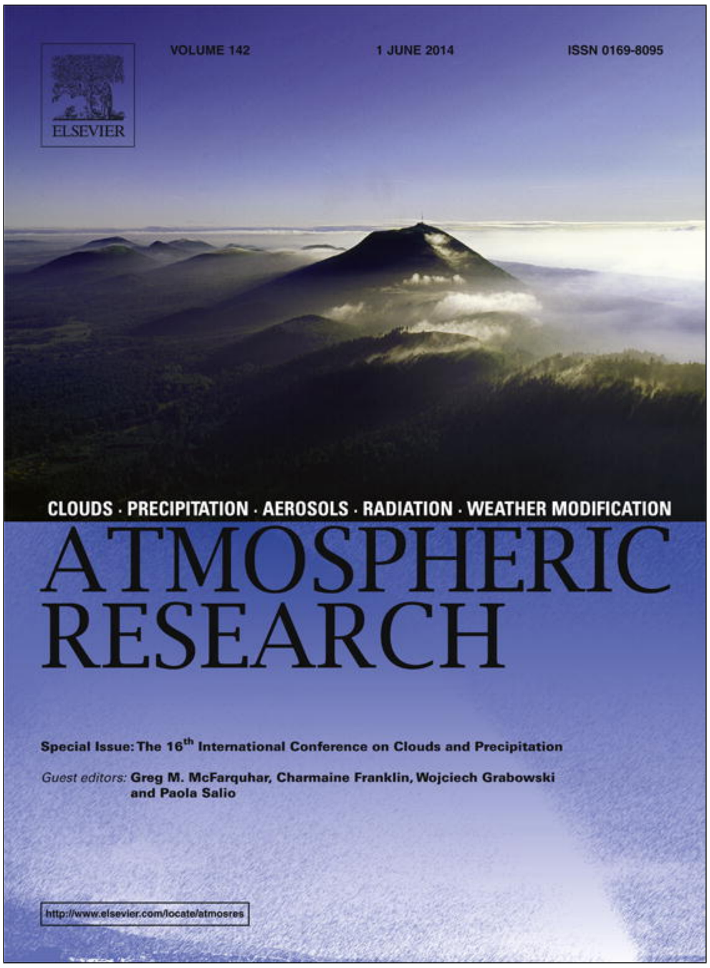
VOLUME 142
1 JUNE 2014
ISSN 0169-8095
ELSEVIER
CLOUDS · PRECIPITATION · AEROSOLS · RADIATION · WEATHER MODIFICATION
ATMOSPHERIC RESEARCH
Special Issue: The 16th International Conference on Clouds and Precipitation
Guest editors: Greg M. McFarquhar, Charmaine Franklin, Wojciech Grabowski and Paola Salio
http://www.elsevier.com/locate/atmosres

Atmospheric Research 142 (2014) 158–170

Contents lists available at ScienceDirect

Atmospheric Research

journal homepage: www.elsevier.com/locate/atmos

Sub-micrometer salt aerosol production intended for marine cloud brightening

Armand Neukermans [a], Gary Cooper [a,*], Jack Foster [a], Alan Gadian [b], Lee Galbraith [a], Sudhanshu Jain [a], John Latham [c], Bob Ormond [a]

[a] FICER, 1225 E. Arques Ave., Sunnyvale, CA 94085, USA
[b] NCAS, Room 11:110, Environmental Sciences, University of Leeds, Leeds LS2 9JT, UK
[c] MMM Division, NCAR, P.O. Box 3000, Boulder, CO 80307, USA

ARTICLE INFO

Article history:
Received 8 March 2013
Received in revised form 30 October 2013
Accepted 31 October 2013

Keywords:
Nanoparticles
Supercritical
Salt
CCN
Geo-engineering
Solar Radiation Management
Marine Cloud Brightening

ABSTRACT

This paper is largely concerned with research focused on, but not restricted to, aspects of Marine Cloud Brightening (MCB), one of several geo-engineering ideas for reducing the amount of sunlight arriving at the Earth's surface, thereby compensating for global warming resulting from fossil-fuel burning. Predominant attention is given to the development of techniques for generating sprays of sub-micrometer salt particles that can enter marine stratocumulus clouds and increase their albedo, thus producing a cooling. Generation of sub-micrometer salt particles by spraying salt solutions at supercritical conditions is described, along with a description of the apparatus used. Log-normal particle size distributions having median diameters of 32 to 286 nm, with GSDs (Geometric Standard Deviations) around 2, were generated by two variations on the technique.

1. Introduction

Marine Cloud Brightening (MCB) is one of several Solar Radiation Management (SRM) ideas designed to produce a global cooling to roughly balance the warming resulting from fossil-fuel burning.

A significant number of papers (e.g., Latham, 1990, 2002; Bower et al., 2006; Salter et al., 2008; Latham et al., 2008, 2012a,b; Rasch et al., 2009; Jones et al., 2009, 2011; Korhonen et al., 2010; Bala et al., 2010) have been published on MCB, which is based on the idea that the albedo of maritime stratocumulus clouds, and possibly their longevity, can be substantially enhanced (Twomey, 1977; Albrecht, 1989) by seeding the clouds with salt or seawater aerosol particles, which are activated as Cloud Condensation Nuclei (CCN), so as to increase the cloud droplet number concentration, N. Seawater aerosol or salt particles would be produced at or near the ocean surface beneath selected clouds and turbulence would cause a high fraction of them to rise into the clouds and become activated to cloud droplets. GCM (General Circulation Model) computations indicate that this geo-engineering technique could produce a cloud albedo enhancement and negative forcing sufficient to maintain the Earth's average surface temperature and polar sea-ice coverage at approximately current values, at least up to the CO_2-doubling point.

One concern that has rightfully been raised regarding deployment of any of the SRM geo-engineering techniques that is capable of creating significant global negative forcing, is that if the technology breaks down, or has to be terminated because it produces unresolvable negative consequences, a major global-scale warming will rapidly be produced. It would therefore be sensible, if SRM deployment is ever deemed to be necessary, to have at least two such techniques acting in concert, so that (hopefully) the remaining technique(s) could be ratcheted up in order to eliminate the possibility of sudden temperature rise. Computations indicate that both the stratospheric sulfur seeding geo-engineering technique

---

* Corresponding author.
E-mail address: sylvrlynyng@gmail.com (G. Cooper).

0169-8095/$ – see front matter © 2013 Elsevier B.V. All rights reserved.
http://dx.doi.org/10.1016/j.atmosres.2013.10.025

(Crutzen, 2006) and MCB–if they are found to function as predicted in GCM modeling studies–could maintain the global average surface temperature at roughly current values until at least the CO_2-doubling point, which may not be reached for several decades. So the two techniques acting in parallel could perhaps buy sufficient time for a clean form of energy to take over, globally, from fossil-fuel burning. An additional possible advantage of having the two techniques deployed at the same time is that fine-tuning (using the sub-global flexibility associated with MCB) should be possible for a significant time.

In our view MCB, and any other SRM technique, should never be deployed unless its usage is approved and deemed to be necessary by a yet-to-be-formed fully international panel representing all countries. It would be vital for a comprehensive examination of all techniques under consideration to be conducted and to accept only those that would not create unacceptable consequences that could not be fully resolved in advance of deployment.

There exist several unresolved questions regarding MCB. For example: (1) GCM modeling assumes a more simplistic picture of these clouds than is warranted, and more complex models need to be developed; (2) It is vital to determine whether undesirable consequences of MCB seeding exist. If they do, and if they cannot be eliminated, then work on this idea should be abandoned; (3) there still exist some technical problems that need to be definitively resolved, particularly in relation to the development of a spray device for producing, in copious quantities, sea-salt or sea-water aerosol particles.

We present herein 1) a discussion of the theory behind a novel technique, 2) a description of an experimental apparatus based on that theory, and 3) results of experiments using the apparatus for the production of salt aerosol of the size-range and particle flux required for effective utilization of MCB, should that ever be warranted. The technique could also be of significant value in aerosol studies, both in the laboratory and in the field.

2. Theory

2.1. Particle size

In simplified terms, in order for seawater aerosol particles to function as CCN and convert into cloud droplets, they must contain a minimum salt mass, which is a function of the supersaturation observed in the cloud, as calculated by the Köhler equation. The average supersaturation in marine stratocumulus clouds is a matter of discussion and various observations, but is estimated to be on the order of 0.5% (Hudson, 2009).

Based on this simplified consideration, one would estimate the minimum salt mass to be on the order of 7×10^{-20} kg (as sodium chloride). Using a seawater density of 1.02 and a salt concentration of 3.5% (mostly sodium chloride), one calculates a minimum initial spray droplet diameter of approximately 160 nm. Using the density of sodium chloride (2165 kg/m^3) the minimum salt mass corresponds to a dry salt sphere approximately 40 nm in diameter.

In practice, the injected aerosol will be competing with a variety of background aerosols including those from air pollution and natural sources, and it is found that suitable nuclei should have minimum diameters ranging from 40 to 100 nm (dry basis), depending on ambient conditions. These correspond to initial spray droplet diameters of 160 to 400 nm.

The practical implementation of CCN production at the suggested scale of 10^{17}/s per source (Salter et al., 2008) has yet to be realized. The required droplet size and number is well beyond the reach of any conventional spraying technology. Additionally, it is thought that the size distribution should be relatively narrow in order to reduce the range of fall-speeds and thus the efficiency of coalescence, leading to longer cloud lifetimes.

The most straightforward way to produce small droplets in a relatively narrow size distribution would be to make use of the Rayleigh jet formation with acoustic-controlled breakup (Rayleigh, 1878), where liquid jets are formed by forcing liquid through small orifices. Such methods require very little energy, and can produce almost mono-disperse droplets if the jets are stimulated at the right frequency, provided coalescence can be avoided (Neukermans, 1973). In such a process one finds that the diameter of the droplets formed is approximately 1.89 times the diameter of the orifice. For example, using holes of 0.4 μm in diameter one might produce droplets on the order of 0.8 μm in diameter (a bit smaller if the jets contract upon exiting the orifice), the size proposed by Salter et al. (2008). Such small holes are relatively easy to fabricate with modern etching techniques. However, the technical challenge lies not as much in fabricating such holes, as in keeping them open during operation. Our efforts in keeping 0.5-μm holes open over extended periods were unsuccessful, even using continuous polish-filtering of the liquid. The amount of liquid sprayed to produce 10^{17}/s nuclei through 0.4-μm holes would be on the order of 30 L/s. Spraying this amount of liquid from a single source is bound to give rise to substantial evaporative cooling of the surrounding air, which could impede the rise of the nuclei into the clouds.

We have looked at alternative droplet formation methods which, while requiring more energy, suffer less from evaporative cooling. Since the volume of the liquid to be sprayed increases with the cube of the droplet diameter one can reduce local evaporative cooling by producing the smallest useable droplet. We have described these efforts in a previous publication (Cooper et al., 2013). The most promising method is probably the formation of Taylor cone jets from seawater, which fortuitously produces relatively narrow size distributions of salt particles with median distribution diameters of 60–85 nm. However, in order to produce 10^{17}/s particles this method would require the formation of at least 10^8 Taylor cones. The creation of a spraying structure with such a number of emitters is an undertaking that is obviously not trivial. We describe here an alternative method, which while requiring substantially more energy, and producing wider distributions, is perhaps easier to implement for research purposes.

The formation of small droplets is impeded by the surface tension of the liquid, as surface energy needs to be provided when the increased surface area of small droplets is created. Intuitively, it can be seen that low fluid surface tension is desired if the liquid is to be dispersed very finely. In more quantitative terms, for the injection and dispersion of liquids, the following relationships are observed (Abraham, 2009):

$$SMD = C\frac{\sigma_l \mu_l^{1/m} \rho_l^{1/n}}{V_l^2 \rho_g} \qquad (1)$$

where:

$$V_l = C_v\sqrt{{}^{2(P_l-P_g)}\Big/_{\rho_l}}. \tag{2}$$

Where SMD = droplet Sauter Mean Diameter, C is an empirical constant, σ_l = surface tension of the liquid, μ_l = dynamic liquid viscosity, ρ_l = liquid density, V_l = injection velocity, ρ_g = gas density, P_l = liquid pressure, P_g = gas pressure, and C_v = orifice flow coefficient.

Reducing the liquid surface tension, increasing the driving pressure and, to a smaller degree, reducing the liquid viscosity and density all reduce the droplet size. The exponents for viscosity and density dependence are small ($m = 2$, $n = 10$). The formula suggests an almost inverse linear dependence on the driving pressure.

Decreasing surface tension is seen to be the most important factor in producing very fine droplets. It is for this reason that raising seawater to temperatures and pressures above the critical point, giving a supercritical fluid where no distinction between gas and liquid exists and surface tension is nonexistent, appeared attractive for the formation of superfine salt aerosols. We discuss theory and describe an experimental apparatus and experiments involving the spraying of solutions of NaCl at various concentrations, in the supercritical regime, through simple nozzles.

2.2. Supercritical salt water

As water is heated at its critical pressure, it is found that its surface tension continuously decreases and eventually becomes zero at the critical point (about 374 °C and 221 bar), where there is no longer a liquid/gas interface. Likewise, it is found that its viscosity also drops very substantially and approaches that of a gas. The behavior of water in this form is almost like a gas although one of high density. One might expect that water in this condition will also spray like a gas.

Another property of water relevant to this discussion is its enthalpy as a function of pressure and temperature. The enthalpy of water is practically unchanged by the addition of small amounts of salt, and hence the enthalpy of pure water is taken to be representative of that of the salt solutions that will be sprayed. The enthalpy of water increases with temperature and decreases with pressure, the latter being somewhat counter-intuitive.

The behavior of water containing salt is very different from that of pure water in the supercritical regime, particularly because of the possibility of phase separation. The properties of seawater at high temperature and pressure have been extensively studied by Bischoff and Pitzer (1989) due to its importance in seafloor geothermal systems. It is found that the critical point is a function of the salt concentration of the water. That is, there is not a single critical point, but a locus of critical points depending on the salt concentration. Both critical temperature and pressure increase substantially with increasing salt concentration. The critical point for a 3.2 wt.% sodium chloride solution is 407 °C and 298 bar.

Since the particular experimental apparatus described here (see below) operates in an almost isobaric mode, it is convenient to plot concentration data at constant pressure as a function of temperature, as shown in Fig. 1.

For the isobaric cross-sections as illustrated, critical points are defined as the minimum of the convex curves. At this point on an isobar curve, vapor and liquid have equal density and are indistinguishable. The part of the curve to the left of the minimum is referred to as vapor phase, while that to the right is referred to as liquid phase. Both of these phases have densities quite different from what is usually associated with these terms.

At high enough temperatures, but outside the isobar curve only one phase is present, namely liquid, although akin to supercritical water, with all salt in solution. For temperatures above the intersection with the isobar, phase separation is observed, and the fluid splits into a vapor phase of low salt concentration, and a liquid phase of much higher salt concentration (a brine).

To illustrate what happens during the isobaric (300 bar) heating process, consider a 1% salt solution. Since the liquid does not change wt.% concentration during heating its representation in the phase diagram of Fig. 1 can be given initially as a vertical line (isopleth). The incoming fluid stays entirely in liquid form until it reaches about 410 °C, the crossing point of the 300-bar single phase line. During this initial trajectory, the density of the liquid decreases substantially, just as happens during the heating of pure water.

At 410 °C, a second phase appears—a brine with a concentration of 6.8% by weight of salt. If the temperature is further increased above 410 °C, the concentrations of the two separate phases will be found at the intersections of the isobar line with the relevant constant temperature line, and will result in a vapor of decreasing salt concentration (left intersection) and a brine with increasing salt concentration (right intersection). For example, at 420 °C it can be seen that the concentration of salt in the vapor decreases to 0.31%, while the brine concentration increases to 20.6%. It will be shown that most of the salt appears in this brine.

Likewise, consider a 3.2% saltwater solution, heated at 300 bar. As can be seen from the curve, this concentration line intersects the minimum of the 300 bar curve and thus defines the critical point for this concentration. From Fig. 1 the critical temperature is found to be 407.5 °C. The fluid is still a single phase when it reaches that critical point, with a density of 0.457, considerably lower than its starting density. If the temperature is raised above 407.5 °C, for example to 420 °C, the single phase will convert into two phases: a vapor of 0.31% salt concentration and a liquid of 20.6% salt concentration (these are the values at the intersections of the isobar curve with a horizontal line at 420 °C).

With increasing temperature, the salt initially in the vapor phase will rapidly partition into the liquid phase. Bischoff and Pitzer (1989) derived equations for the mass fractions of vapor, X_V, and liquid, X_L. The equations may be extended to allow calculation of the volume fraction of vapor and liquid and the salt mass fraction in the same.

For the 3.2% saltwater example from above, at 420 °C, where the vapor salt concentration $S_V = 0.31\%$, and the brine salt concentration $S_L = 20.6\%$, the equations give the mass fraction of the liquid $X_L = 0.142$, and the mass fraction of the vapor $X_V = 0.858$. Most of the total mass is in the vapor.

Using $\rho_L = 0.788$ and $\rho_V = 0.203$ (Bischoff, 1991) the equations give the volume fraction of the liquid $Y_L = 0.041$, the volume fraction of the vapor $Y_V = 0.959$, the salt mass

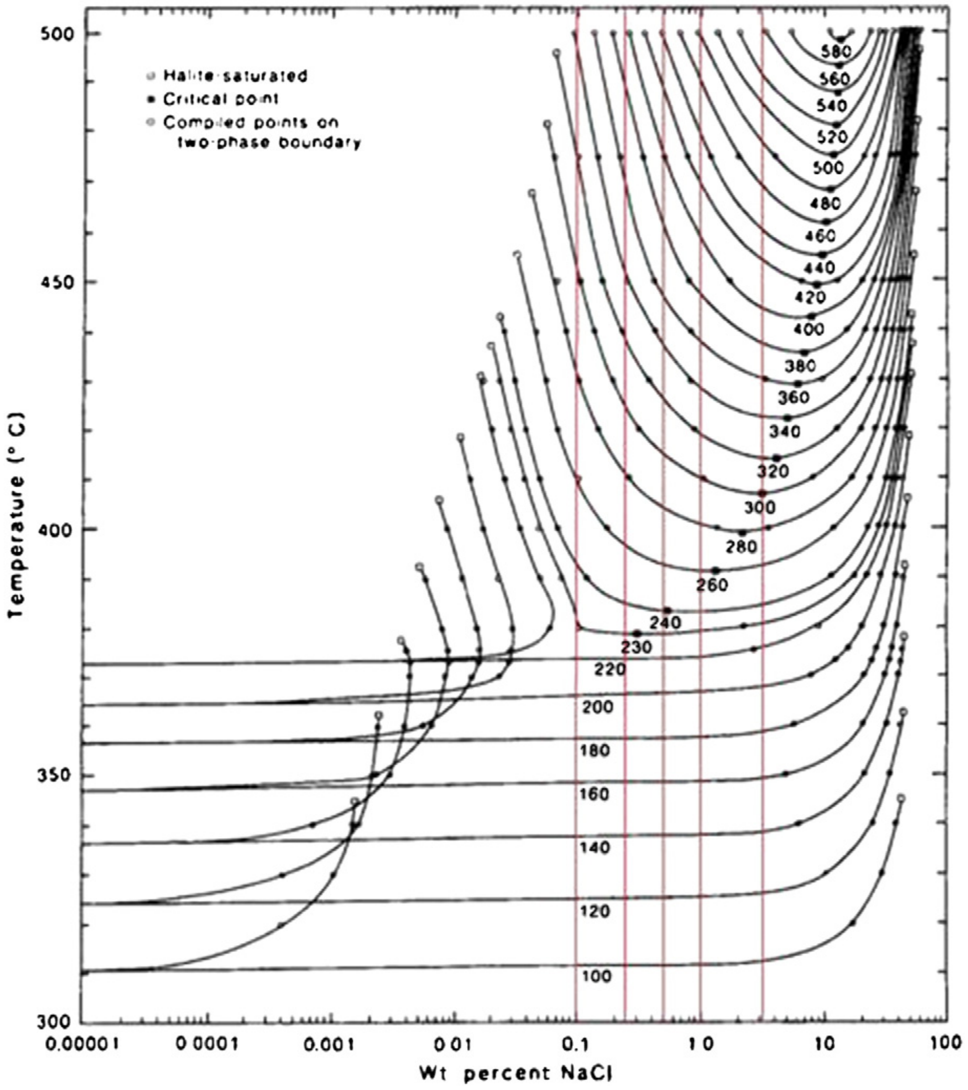

Fig. 1. Isobars of the vapor–liquid region of NaCl–H_2O solutions from 100 to 580 bar, as a function of the salt concentration in wt.% and temperature in °C, with 3.2%, 1%, 0.5%, 0.25%, and 0.1% isopleths added (adapted from Bischoff and Pitzer, 1989; reprinted by permission of the American Journal of Science). These vertical lines represent isobaric heating trajectories for incoming liquids.

fraction in the liquid $Z_L = 0.914$, and the salt mass fraction in the vapor $Z_V = 0.086$. Thus, on moving into the two-phase region most of the mass and volume of the original solution remain in vapor form, but most of the salt mass goes into the liquid phase.

For a given salt concentration, at the temperature where the vertical line just intersects the isobar to the left of the minimum, the liquid mass fraction is zero. This would appear to be an ideal operating point for spraying, with all the salt being entirely in the single vapor phase. This intersection defines the maximum temperature at the selected pressure where a single phase exists. For a fixed concentration, selecting various pressure curves along the vertical line yields various intersection temperatures, and these points, when plotted in a P–T diagram yield the boundary between the one phase and two phase regimes.

Fig. 2 shows the loci for 3.2%, 1%, 0.5%, 0.25%, and 0.1% NaCl solutions on a P–T plot. These curves delineate the separation between the one phase and two phase regimes. Directly above any point on a curve (increasing pressure) a single phase exists, and directly to the right of it (increasing temperature) two phases exist. Also drawn in this representation is an isenthalp of 2676 kJ/kg, which has been found to play a critical role in successful spraying, and will be discussed below. Not shown in Fig. 2 is a lower phase separation line that defines the precipitation of solid salt (halite, a third phase) that occurs when the brine concentration exceeds about 40%, at the extreme right end of the isobars of Fig. 1.

3. Description of the experimental apparatus

3.1. Summary description

A schematic of the conceptually quite simple apparatus built to heat and spray saltwater through a small orifice is shown in Fig. 3. It comprises water reservoirs, a pump, a pressure gauge, a serpentine heating tube enclosed in a block heater, and a nozzle enclosed in a separate block heater. The apparatus is designed such that at the desired orifice flow rate, the fluid exit temperature can reach the desired value by controlling the temperature of the heating block. As it flows through the tube

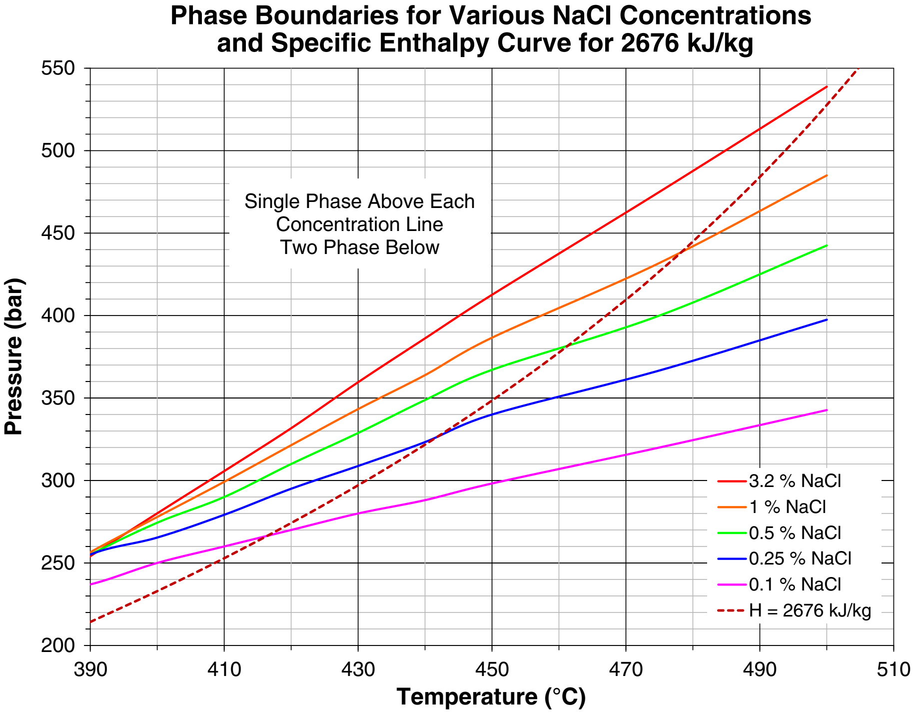

Fig. 2. P–T plots of phase boundaries for various NaCl concentrations (data from Bischoff and Pitzer, 1989) and the specific enthalpy of saturated steam (data from Lemmon et al.).

under pressure the fluid is gradually converted from its incoming liquid state at ambient temperature to a supercritical fluid somewhere near the exit. At the same time, the fluid experiences a substantial decrease in density, and therefore an increase in velocity, and undergoes changes in many physical characteristics that effect heat transfer characteristics. Save for the small pressure drop created by the flow, the fluid is under constant pressure.

3.2. Pressure and flow considerations

Because of the high temperatures and pressures that are employed, operating safety is a primary concern. After preliminary experiments using a high pressure reservoir pressurized with nitrogen to drive the flow, a pneumatic-driven positive displacement pump was selected. The high pressure fluid is liquid until it gets heated above criticality near the output end of the serpentine tube. The total volume inside of the small diameter metal tube stores a minimal amount of energy as high pressure fluid.

Two liquid reservoirs, one containing saltwater and the other containing distilled water are connected alternately with a two way valve to the pump inlet. This allows the use of pure water to flush out the system at the start and end of an experiment to remove any salt residue and thus reduce chloride-induced corrosion of the components while not in use. The Haskel Model SF-60 pump uses compressed air on a large piston to drive a small piston that pumps the liquid, giving a pressure boost of 69:1.

Spring-loaded check valves with low cracking pressure maintain the pump output pressure during the brief periodic refilling of the pump's fluid cylinder, which has a capacity of 11 mL. The laboratory compressed air that powers the pump is buffered by a spare compressor tank on a “Tee” to the supply line just before the pump in order to minimize transients in the supply pressure, and maintain adequate air flow, during periodic pump refilling. Given the known stroke volume, the measurement of the time interval between strokes provides for a reliable measurement of the fluid flow, averaged over the duration of the stroke (typically on the order of 1 min).

During retraction of the piston (refilling), there is a momentary drop in pressure of as much as 10% of the nominal value, as the check valve lags in closing for a fraction of a second. If the operating point (pressure and temperature) is at the one-phase boundary, then this drop in pressure moves the operating point into the two-phase region, allowing the formation of a liquid brine as described above. While the excursion to lower pressure is a small fraction of the pump duty cycle (a fraction of a second versus approximately 1 min for a full 11-mL delivery), this is apparently enough to create significant amounts of brine. It is particularly a problem when the temperature of the heated tube wall is significantly higher than that of the bulk of fluid that is in supercritical condition (near the end of the heating tube). Swept out of the tube, the brine interferes with the formation of narrow particle size distributions. Brine formation is manifested mostly as discontinuous “spitting” of bursts of larger particles from the nozzle.

The most obvious solution to this problem would be to include a pulse damper, so as to decrease the pressure excursions. However, the very large buffer volume of the available dampers compared to the miniscule flow rate makes it impossible to flush the damper in a reasonable time when transitioning from saltwater to pure water and vice versa, leaving the effective salt concentration unknown. Note that during operation the end of the tube is filled with supercritical fluid that is compressible and therefore acts to some degree as a damper itself, although a relatively small one. Eventually two Haskel pumps were used in parallel, one acting as the main

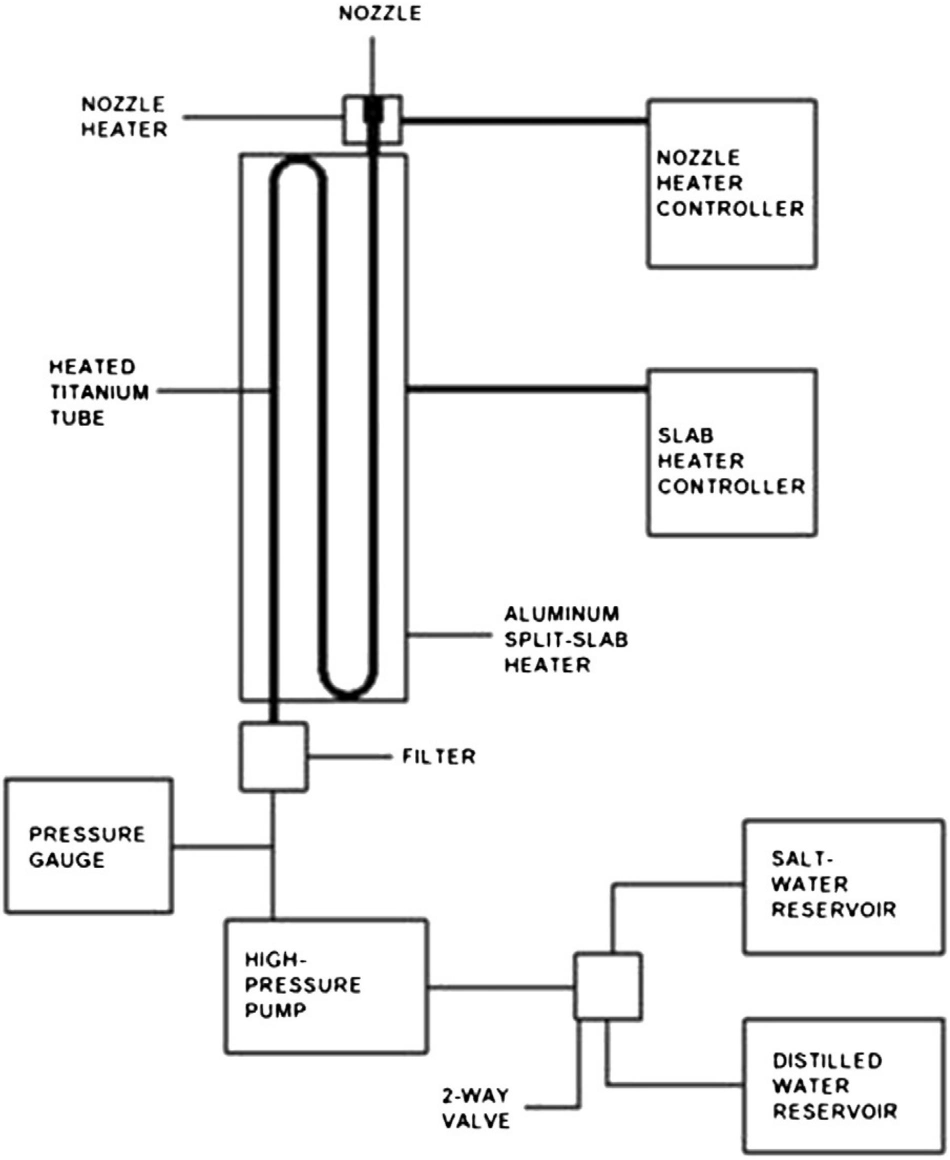

Fig. 3. Schematic of the supercritical spray apparatus used to produce nanometer-sized NaCl particles.

operating pump and the other as a feeder pump. The feeder pump is set at a delivery pressure very slightly below the operating pressure of the operating pump. While the piston of the operating pump is retracting, the feeder pump supplies the makeup liquid instantly. With this setup it was found that pump system pressure transients could be reduced by about a factor of five at operating pressure with supercritical fluid (and by a factor of ten when only non-compressible liquid is present).

Another way to mitigate the problem is to decrease the temperature difference between the tube wall and the bulk fluid such that the tube wall temperature barely exceeds the target temperature at the one-phase boundary. To this end, the outside diameter (OD) of the operating tube was sequentially decreased from 6.35 mm to 3.18 mm, and eventually to 1.59 mm (0.51 mm inside diameter (ID)). As will be demonstrated in Appendix A, this increases the Reynolds number of the flow from a value of 1000 to well over 8000 reducing the temperature difference between the wall and the bulk of fluid from 7 to 0.25 °C. The high Reynolds number ensures fully developed turbulent flow. At the same time the higher flow velocity in the narrower tube may help to flush out any brine before it can accumulate and produce the periodic “spitting”.

A nozzle with an orifice of typically 50 μm in diameter is connected with fittings at the hot end of the titanium tube. To maintain the fluid temperature right up to the expansion, and to heat the air in its immediate vicinity, the nozzle and fittings are heated by another split-slab heater made of aluminum. Due to the Joule–Thomson effect, the nozzle is cooled very rapidly without a heater block. Experiments have demonstrated the importance of this extra heater in achieving good particle size distributions.

An electronic pressure gauge (Ashcroft 45 302074SD02L) was used to measure the exit pressure of the pump. An inlet filter (Nupro SS-47 F-KG-7) removed all particles larger than 15 μm.

3.3. Materials of construction

Supercritical water is very corrosive, and supercritical saltwater even more so. In this application the problem is magnified by the fact that loose corrosion products can obstruct the small orifice of the spray nozzle and therefore physically interfere with spraying. The spray-nozzle orifice in particular, being at high temperature and pressure and very significantly stressed, presents an additional stress-corrosion problem. Stainless steel and nickel alloys were found entirely unsatisfactory for this application. They are satisfactory for those parts of the tubing that are not heated.

Type 2 titanium proved to be the most corrosion resistant material for this application, but 1.59-mm OD tubing of this grade is difficult to source, particularly in the small quantities needed. While this tubing proved entirely satisfactory for pure water, the addition of even a small percentage of salt causes the leaching of a brown substance that tends to deposit inside the nozzle, creating an obstruction and a gradual decrease in flow rate. Analysis of the deposit by XES (X-ray Energy Spectroscopy) revealed that it comprises mostly iron, a common contaminant in titanium and its alloys, present at up to 0.2% in Type 2 titanium. While it might be expected that it would leach from the surface and be depleted over time, at the high operating temperatures employed here, diffusion from the bulk appears to be sufficient to replenish it, thereby creating an ongoing problem.

Application of inert coatings such as titanium carbide, titanium nitride, or diamond-like carbon to surfaces exposed to supercritical saltwater was considered, but these materials are difficult to apply to the inside of a very narrow tube well over a meter long. Therefore to improve the inertness of the tubing, a very thin layer of gold was applied to the inside of the tube. This was achieved by forcing a diluted organic gold solution (Englehard Industries, Hanovia Liquid Gold Div, E. Newark, NJ; Bright white gold #1) through the tubing with a syringe. The resulting fluid coating adhering to the inside wall was then carefully blown dry and subsequently heated very slowly to above 500 °C with continuous airflow through the tube, decomposing the organic structure and leaving a thin metallic layer of gold. Similar treatment to the outside of the tubing provided a very durable and strongly adhering coating. Application of this technology provided a dramatic, but not yet complete, reduction of the corrosion clogging problem, possibly due to coating defects.

As mentioned above, stress corrosion caused by a combination of high temperature, pressure and high localized stresses is particularly intensive at the nozzle orifice. A variety of nozzle materials such as Monel®, titanium, and ceramics such as silicon carbide and sapphire were studied. The lifetime of a sapphire nozzle was typically a half hour during which time the size of the orifice doubled. The only suitable material found so far is diamond, either in natural or synthetic form. Natural diamond nozzles with 50-μm diameter orifices, used in water jet cutting mills, were obtained from Diamond Technologies Inc. Synthetic diamond, in sheets of 300 and 400 μm thick, was a gift from sp3 Diamond Technologies Inc. The latter were laser cut and drilled to the desired shape using a Samurai UV Laser Marking System courtesy of DPSS Lasers, Inc.

The diamonds were seated in a titanium holder, held in place and sealed with a variety of materials. Given the large difference in expansion coefficient between diamond and titanium (ca. 1 ppm/°C versus 9.5 ppm/°C) leak-free sealing at high temperature is difficult. Diamonds were successfully brazed to the titanium holder, but in operation the brazing alloy was rapidly attacked by the solution, and this approach was abandoned. Satisfactory results were obtained using circular gold wires or laser drilled circular 0.25-mm thick gold foils as sealing gaskets. The best approach is simply to press-fit the diamond at high temperature into a fitted opening in the titanium holder.

The most vexing experimental problem proved to be the making of non-leaking connections between the tube and the nozzle. There are no suitable small commercial tube connectors rated at both these pressures and temperatures. Swagelok® titanium tube connectors, Valco titanium components made for high pressure liquid chromatography, and custom-made titanium connectors with 0.5-mm bores (courtesy of Current EDM, Inc.) were tried with intermittent success. Since the working spray orifice is very small (50–100 μm) even a very small connector leak may have a significant effect on the spray. Leaks, buried inside the heater block or behind glass wool insulation, are difficult to detect. Often their location is such that they can preferentially remove condensed brine formed at the tube walls, the result being a narrower size distribution of particles than if the fluid had emerged only from the nozzle.

3.4. Spray medium

All experiments have been conducted with solutions of reagent grade sodium chloride in distilled water rather than with seawater. This is because the divalent ions in seawater, principally magnesium, calcium and sulfate, would precipitate as calcium sulfate and magnesium hydroxide sulfate on warming above about 350 °C (Bischoff and Rosenbauer, 1983), depositing on tube surfaces and potentially clogging nozzles. The P–V–T properties of 3.2% sodium chloride coincide exactly with those of seawater, within experimental error, over the ranges 200–500 °C and 100–700 bar (Bischoff and Rosenbauer, 1985). If seawater is to be used in future implementations, reverse osmosis and ion-selective membrane treatment (a technology well-known in the oil industry) will most likely have to be employed to remove these ions prior to spraying.

3.5. Sampling and analysis

No optical instrument capable of directly analyzing the spray of small particles (20–200 nm equivalent sphere diameter) from the apparatus was available. However, observation of the emerging plume by forward scattered light provides for a surprisingly good quantitative monitor. As the size of the emerging particles is changed from micron-sized to 100 nm or below, the color of the obliquely scattered light changes from white to blue, as seen in the digital camera images in Fig. 4a and b, and eventually almost disappears. Even observations of the backscatter of the beam of a green laser pointer through the particle cloud were found to be predictive of spray quality.

For quantitative measurements, a simple electrostatic precipitator was constructed. The spray enters a collection hood with a HEPA filter and suction blower on the top. The suction blower was operated continuously during spray operation, but was stopped when it was desired to collect a sample for analysis. The electrostatic precipitator, with a negatively charged wire-grid corona ionizer, employed a small suction fan to draw aerosol from the collection hood into the precipitator and onto a 2 or 3-inch silicon wafer at ground potential.

The salt particles collected on the silicon wafer are (mostly) cubic crystals that appear to be dry upon arrival at the wafer under normal spraying conditions. The silicon wafer samples were scanned with a Hitachi Model 4160 Scanning Electron Microscope (SEM) at the Stanford Nanofabrication Facility (SNF). 2-D processing using a despeckling median filter and analysis of the digital SEM images using the public-domain software package Image-J, developed by Wayne Rasband at NIH, gave a list of particle surface areas that was further analyzed using a spreadsheet to calculate log-normal distribution median diameters (of spheres of equivalent volume to the assumed cubic salt particles) and the Geometric Standard Deviation (GSD) of the distributions.

3.6. Thermodynamic and flow considerations

Given the very fast transit of a fluid parcel through the spray orifice (microseconds) the transition may be considered adiabatic, and neglecting the relatively negligible fluid velocities away from the nozzle, the transition from working pressure to atmospheric pressure may therefore be considered to conserve enthalpy.

Somewhat surprisingly, expanding pure water at its critical point (about 374 °C and 221 bar) to atmospheric pressure results in the formation of wet steam (a mixture of water vapor and water droplets). This is because at the critical point water does not possess enough enthalpy for complete evaporation. The specific enthalpy of dry saturated steam is 2676 kJ/kg, and that of water at its critical point is only 2032 kJ/kg.

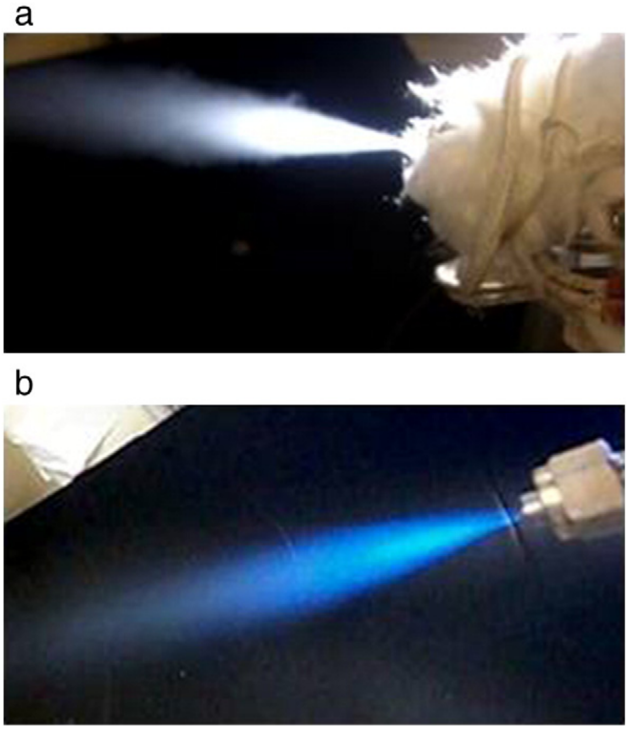

Fig. 4. Saltwater spray illuminated with white light. The white plume in the top image is due to micron-sized particles while the blue color in the bottom image is due to Rayleigh scattering of light by nanometer-sized particles.

The isenthalp of 2676 kJ/kg has been plotted in the P–T diagram of Fig. 2. The intersection of this line with the single phase vapor boundary for the selected salt concentration, defines an operating point that satisfies both conditions (the enthalpy may of course exceed the minimum).

It has to be recognized that the criterion above for minimum enthalpy is perhaps a necessary, but not necessarily a sufficient condition to obtain a fine spray distribution. With pure water it is observed experimentally that at the supercritical point the spray plume is white, indicative of the presence of many micron-sized droplets (wet steam). As the conditions of pressure and temperature are adjusted to reach 2676 kJ/kg, the plume is seen to disappear completely, indicating that complete conversion to dry steam has taken place. This provides for an excellent way to set this enthalpy point with pure water, and subsequently change over to saltwater, eliminating all the experimental errors in real fluid temperature measurement. However, this condition by itself does not ensure that the fluid will be optimally distributed into ultrafine drops. In principle, and in fact, the fluid does not need to be fully evaporated to produce excellent particle size distributions.

In practice however, it is observed that these operating points provide good spray conditions, as will be demonstrated in the section below.

As can be seen in Fig. 2, the optimal operating points (pressure and temperature) become rather high for high salt concentrations, and some of them are outside the safe operating region of the experimental setup.

The fluid, at the point of entry into the nozzle, is a single compressible phase. The flow of this fluid through an orifice may therefore be determined by the formulas governing the behavior of compressible flows. Under choked-flow conditions the mass flow rate is given by Eq. (3):

$$m = CA\sqrt{k\rho_0 P_0\left(\frac{2}{k+1}\right)^{\frac{k+1}{k-1}}} \tag{3}$$

where m is the mass flow rate, C the discharge coefficient, A the discharge hole area, k the ratio of the specific heats of the fluid under constant pressure and volume, ρ_0 is the density of the fluid and P_0 the applied pressure (Perry and Green, 1984).

For example, for a 0.5% salt solution at 380 bar and 463 °C, by interpolation of the data of Bischoff (1991), a fluid density of 0.203 is found, and from the NIST tables for pure water (Lemmon et al.) $C_p = 8.74$ J/g·K and $C_v = 2.8$ J/g·K, giving a ratio $k = 3.12$. Through a 50-μm orifice, under these conditions, one calculates a mass flow of 0.128 g/s or 7.7 mL/min, in good agreement with the observed experimental flow of 8 mL/min.

The extremely complicated physical flow phenomenon at the nozzle exit and beyond is briefly discussed in Appendix B.

4. Experimental results

During the development of the process 53 experiments resulted in the collection of 103 salt-on-wafer samples. Thirty-nine of these salt samples were judged to have meaningfully analyzable particle distributions (enough particles to be representative and clear enough images to be analyzed). Many of the 53 experiments, especially the earlier ones, were to some degree compromised by such exigencies as leaks, inability to accurately determine fluid temperature, collection of wet droplets, and inability to obtain meaningful SEM images. For the 39 salt samples, most of the distributions were observed to be approximately log-normal and were fitted that way. The distribution median diameters (d_g) in these experiments ranged from 32 to 286 nm while the GSDs, (σ_g) ranged from 1.48 to 2.61. Half of these observations had a distribution median diameter of 67 nm or less, and a mean GSD of 2.08. Nominal orifice diameters ranged from 50 to 100 μm, with the diameter having little effect on the observed particle size distribution. Partially obstructed nozzles with small effective diameters (31 μm, for example) did however produce smaller particle sizes (34 nm).

4.1. Results from spraying in a single-phase regime

The results most representative of what can be consistently obtained for single-phase spraying, after a considerable learning curve, are shown in Figs. 5 and 6. The operating conditions in Fig. 5 are 462 °C and 379 bar, using a 0.5% salt solution, which is just at the two-phase boundary of the phase diagram for that concentration (Fig. 2).

Applying log-normal statistics to the data yields a distribution median diameter of 57.5 nm, and a GSD of 2.03. Raising the enthalpy slightly to 2750 kJ/kg by changing the operating conditions to 481 °C and 409 bar gives the results illustrated in Fig. 6.

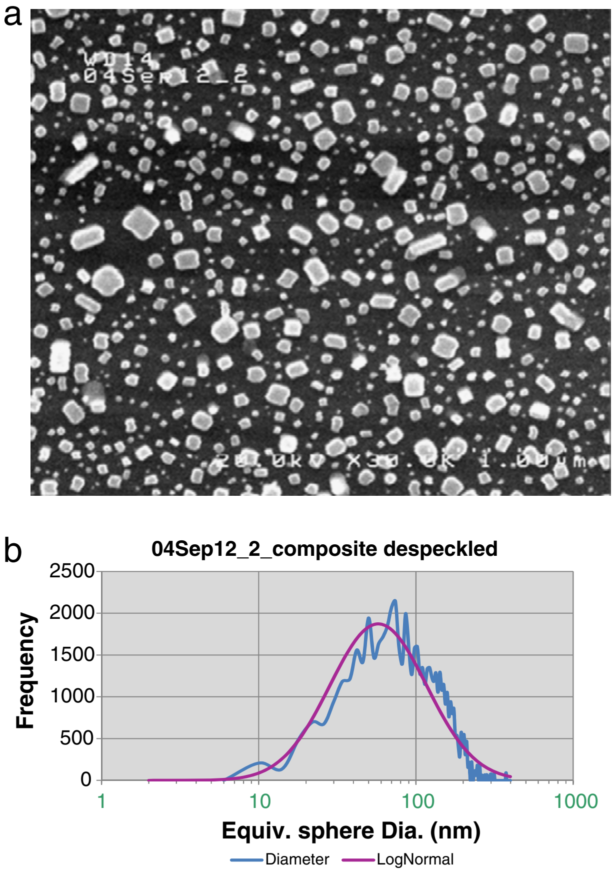

Fig. 5. Salt particle distribution, analyzed by SEM, for an 8 mL/min flow of 0.5% NaCl solution through a 50-μm diamond nozzle at 462 °C and 379 bar, with specific enthalpy of 2676 kJ/kg. The distribution median diameter is 57.5 nm, with a GSD of 2.03.

The distribution median diameter decreases from 57.5 to 45.6 nm. Both higher pressure and higher temperature are conducive to producing smaller droplets, according to classical spray technology (Eqs. (1) and (2)), but a partially clogged nozzle, reflected in a decreased flow rate (6.8 mL/min), may also have had an effect.

These experiments show that operation at single-phase vapor conditions with enthalpy of 2676 kJ/kg or higher will produce nanoparticles with distributions close to those required for the Latham scheme (Latham, 1990, 2002). Comparing the enthalpy of 2750 kJ/kg with 2676 kJ/kg, the diameter is slightly less but the distributions are very similar. The theoretical minimum enthalpy of 2676 kJ/kg is sufficient to give a good particle size distribution in these cases.

4.2. Results from spraying in a two-phase regime

The repeatability, and hence the evaluation of the experimental results in terms of observed particle distributions vs. experimental parameters, was not very good until recently. The measured flow rate often varied due to nozzle orifice clogging. The presence of very small leaks at the connector, endemic at these temperatures and pressures, seems to skew the distribution towards smaller sizes. If any liquid is nucleated, it does so preferentially at the tube wall, where the temperature is higher than in the bulk of the flow. Having low surface tension, it can easily exit through small imperfections at the connector. While this liquid volume may be low, it carries a disproportionate amount of salt, as discussed above in Section 2.2.

When brine was present, the distribution was normally characterized by the addition of large crystals, on occasion giving rise to bimodal distributions. When observed, liquid "spitting" tended to occur explosively, in periods of a few seconds, characterized by the appearance of a momentarily visible white plume, indicating the presence of micron-sized droplets, followed by normal spraying behavior. Sampling however covered typically a few minutes and thus integrated both of these distributions.

In early experiments, when the occasional appearance of the brine phase was not fully understood, salt was sometimes collected during the first few minutes of the spray, without any sign of liquid present, even with the system operating nominally in the two-phase regime. Liquid spitting would not be observed for as much as 10 min of operation. This may have been due to the fact that the location of the transition in the tube to the two-phase regime was close to the nozzle, and nucleation of brine did not occur instantly during the short transit to the nozzle orifice. In the absence of brine the distribution was normally of smaller particles.

An illustration of this effect can be seen in Fig. 7. A 1% salt solution was heated to 395 °C at 260 bar, where it just reached the critical point (top image). Further heating by 10 °C caused a dramatic change, as seen in the bottom image.

This is due to the fact that further heating has moved the system into the two-phase regime, creating vapor of approximately 0.1% salt concentration, and the vapor emerges first, long before the accompanying liquid appears. The distribution as was originally analyzed, with the spray appearing perfectly stable, is in fact not representative of the long term results that may evolve.

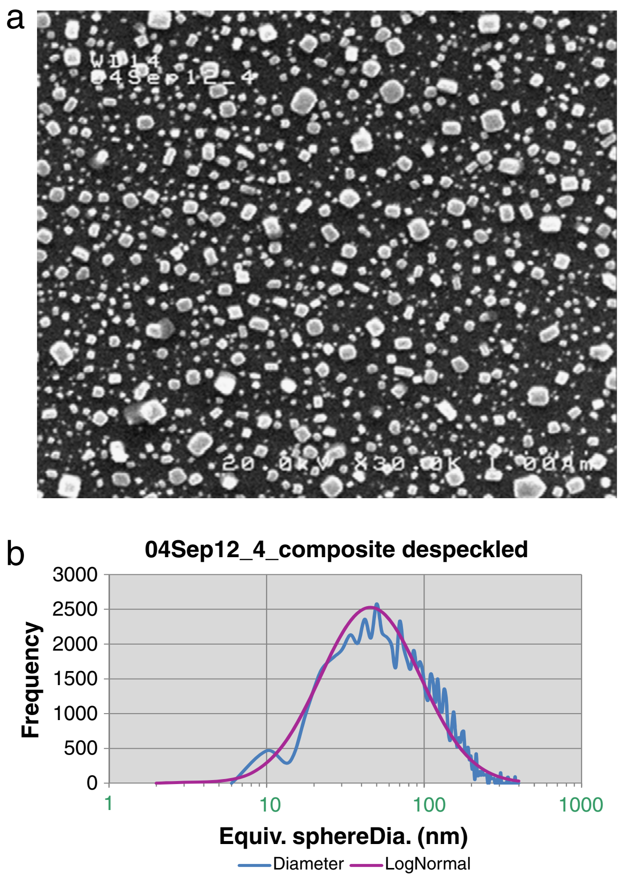

Fig. 6. Salt particle distribution, analyzed by SEM, for an 6.8 mL/min flow of 0.5% NaCl solution through a 50-μm diamond nozzle at 481 °C and 409 bar, with specific enthalpy of 2750 kJ/kg. The distribution median diameter is 45.6 nm, with a GSD of 2.08.

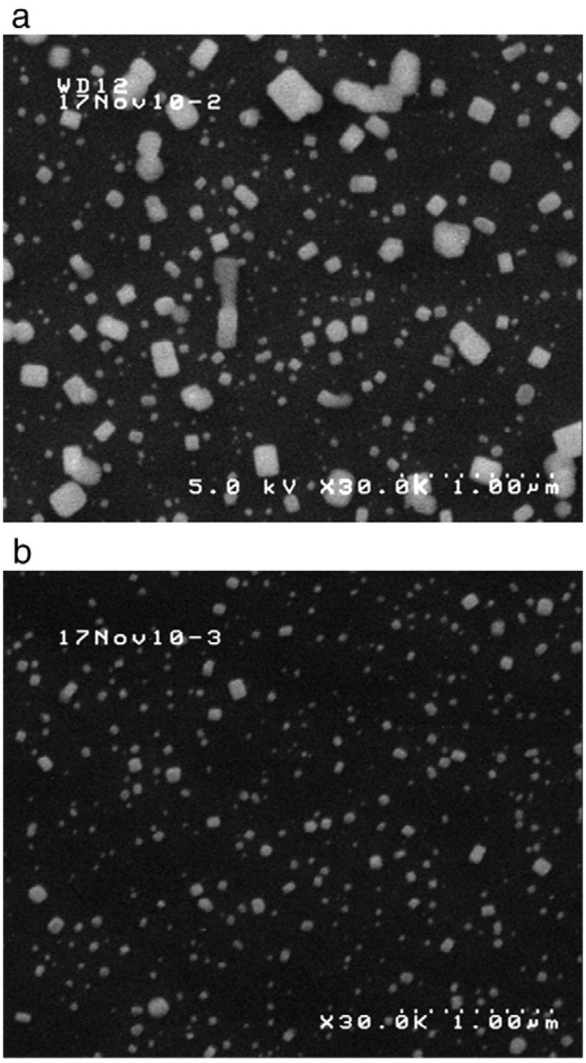

Fig. 7. Salt particle distributions, analyzed by SEM, for a 1% salt solution sprayed at 260 bar and 395 °C (top image) and 405 °C (bottom image). The distribution median diameter decreases from 58 (GSD = 2.17) to 48 (GSD = 1.78) nm, because only the vapor is being sprayed in the latter case.

In principle, tapping off the liquid before it can reach the nozzle provides a means of producing nanometer-sized particles of various diameters from a single salt concentration, simply by modifying the temperature of the spray. As the temperature is raised, its intersection with the vapor section on the isobar moves to lower salt concentrations, providing smaller and smaller particles in the vapor spray, which is experimentally observed.

Fig. 8 shows the salt particles from the vapor-phase spraying of a 3.2% salt solution at 425 °C and 230 bar (well into the two-phase regime).

The simple fabrication of these nanometer-sized salt crystals, while perhaps not suitable for MCB, provides copious laboratory quantities of nuclei, fully dry, in aerosol form, and easily tunable in diameter. This phenomenon may be interesting for general cloud research, and can perhaps be applied to other salts.

5. Discussion of results and conclusions

The efficiency of the supercritical saltwater spray method is bounded on the one side by the ineffectiveness of the smallest particles at the lower end of the distribution to act as CCN, and on the other side by the increasing number of nozzles and amount of energy required if the diameter is increased. For a CCN effectiveness cut-off diameter of 40 nm, 29% of the particles in the distribution of Fig. 5 are ineffective (Fig. 9), while 42% of those in the distribution of Fig. 6 are ineffective. From this perspective the spray seems quite efficient, and overall these distributions look promising.

However, most of the volume or salt mass sprayed is in the tail end of the log-normal distribution, particularly in the case of a large GSD. In this respect, it is instructive to plot the cumulative number and volume distributions, as illustrated in Fig. 9, of the log-normal distribution illustrated in Fig. 5, i.e., median diameter = 57.5 nm and GSD = 2.03.

Particles smaller than 40 nm represent about 29% of the cumulative number, while those smaller than 100 nm represent about 78%, and thus particles with the most desirable diameters (40–100 nm) represent 49% of the number fraction. However, their volume corresponds to only 9.8% of the total volume. Likewise, 50% of the volume sprayed is coming from particles larger than 250 nm, of which there seem to be few if any in the number distribution. It is the number of particles sprayed that is of first order importance, not the volume sprayed, but the efficiency of spraying is determined by how much of the volume is converted to droplets in the desired size range.

For a log-normal particle distribution, the volume distribution is also log-normal, and its characteristics can be derived

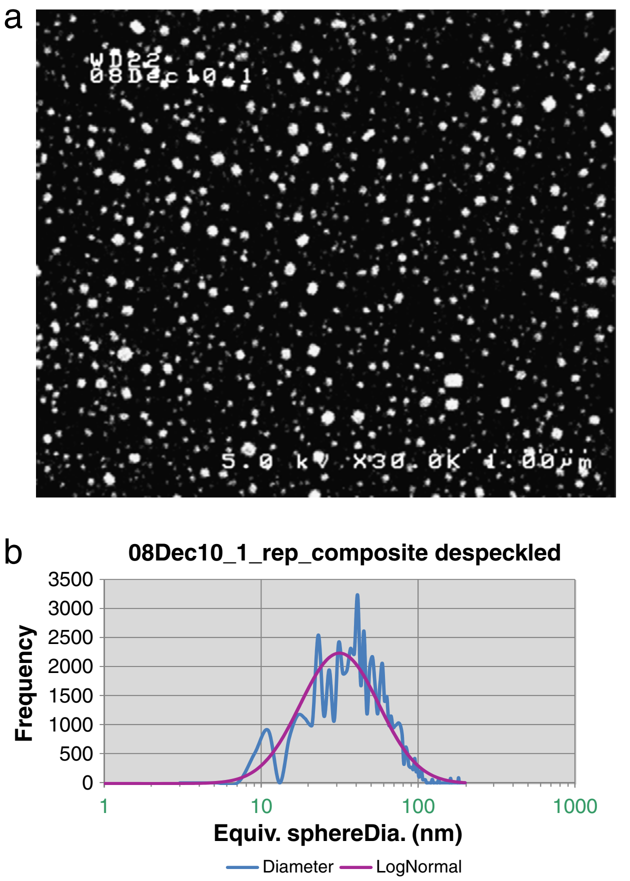

Fig. 8. Salt particles with a distribution median diameter of 32 nm obtained from the vapor-phase spraying of 3.2% salt solution at 230 bar and 425 °C.

from d_g and σ_g. The diameter of average mass or volume is given by $d_v = d_g\exp(1.5\ln^2\sigma_g)$ (Hatch and Choate, 1929). The volume of a particle of diameter d_v, multiplied by the total number of particles, yields the total volume in the distribution. Hence for a given volume sprayed with a known distribution, the number of particles produced can be derived by dividing the spray volume by the volume of the particle with known diameter d_v. For a distribution with a GSD of 2.03, we find $d_v = 2.12 \times d_g$.

Given the flow rate of the nozzle, we can now determine the number of particles produced per second for a given distribution. Assuming a flow rate of 8 mL/min, as in Fig. 5, and a salt concentration of 3.2%, we find a liquid flow of 1.33×10^{-4} kg/s, which yields 4.27×10^{-6} kg/s of salt, or a volume flow of salt of 1.972×10^{-9} m^3/s, given a salt density of 2165 kg/m^3.

Fig. 10 illustrates the number of particles that may be expected from various log-normal distributions for this volume flow of salt, for a variety of assumed median diameters d_g and various GSDs. It is seen that under these conditions, approximately 1.7×10^{12} particles may be expected from one nozzle. Based on a liquid flow of 1.33×10^{-4} kg/s and enthalpy requirement of 2676 kJ/kg, each such nozzle would require 335 W. Only 5 W is mechanical power, and the rest is thermal, in principle an ideal arrangement for a power unit producing a lot of waste heat, as on a ship, although much of the heat that is required is of high quality.

To obtain 10^{17} particles per second, approximately 60,000 nozzles would be required if $d_g = 57.5$ nm, spraying at 7.86 L/s. This would necessitate a total input power of 20.1 MW, the electrical requirement of a small city, obviously an unacceptably large amount. If the spray could be improved by further tuning to a distribution with a GSD of 1.6, the required number of nozzles and power would drop by a factor of 3.5. Distributions with a GSD of 1.6 were observed in a few experiments. Using a d_g of 45.6 nm, as illustrated in Fig. 6, one might reach almost 10^{13} particles per nozzle if a GSD of 1.6 could be achieved. At this point, although these results cannot be reproduced systematically, simultaneous obtainment does seem like an achievable goal. The number of physical nozzles could probably be reduced by a factor of nine (or more) by using 150-μm diamond apertures rather than 50-μm apertures, but this does not reduce the energy requirement. The use of sheets of synthetic diamond, 300–400 μm thick, lends itself well to the fabrication of linear aperture arrays if necessary, using either laser hole drilling or in-situ creation during diamond sheet growth.

Based on these considerations, it would seem more realistic to envision a research test unit producing 10^{16} CCN/s, with some 6000 spray apertures, which might require 2 MW, or perhaps only one fifth of both numbers with further improvements. Multiple spray holes produce much larger flows and require larger tubing. As before, it is highly desirable to maintain high Reynolds numbers (>8000) for heat transfer and to minimize

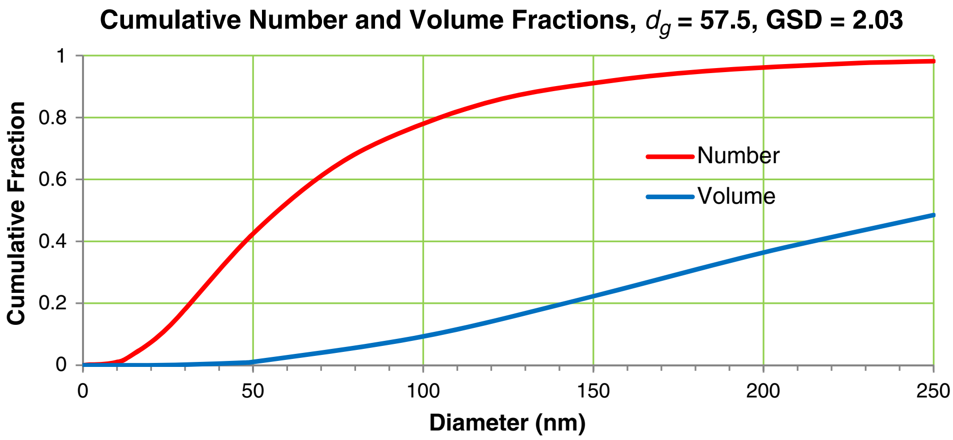

Fig. 9. Cumulative number and volume fractions of the log-normal size distribution of the particles of Fig. 5, with median diameter = 57.5 nm, and GSD = 2.03.

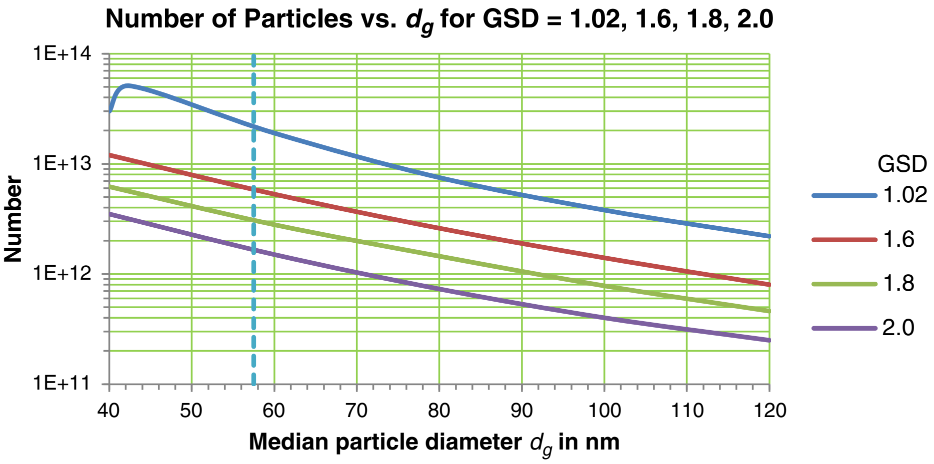

Fig. 10. Number of particles obtained from 3.2% saltwater flowing at 8 mL/min, assuming the distribution is log-normal, for various median diameters (d_g) of 40 to 120 nm, and GSDs of 2, 1.8,1.6 and 1.02 (i.e., essentially monodisperse). The number fraction smaller than 40 nm has been removed from the count.

the temperature difference between the wall and the bulk of the fluid in order to avoid overheating. Preliminary calculations (along the line of the detailed calculations for the present tubing in Appendix A) indicate that a 3.174-mm ID, 5 m long titanium tube would give the desired heating characteristics.

It is seen that the elimination of surface tension in supercritical saltwater can indeed provide for excellent formation of research quantities of salt particles with distribution median diameters as small as 32 nm, tunable in diameter, fully dried and air dispersed, at a rate of on the order of 10^{14}/s, suitable for experimental cloud studies. This can be accomplished by draining off the brine phase (which contains most of the salt in solution) and spraying only the vapor phase, when operating in the two-phase regime. The size tuning is achieved by simply adjusting the temperature. For example, the vapor phase of 0.5% salt solution at 240 bar will produce decreasing size nanoparticles as the operating temperature is raised from 385 to 450 °C, because the salt concentration in the vapor decreases by a factor of 20 over that temperature range. The diameter (d_g) of the salt particles may change from 100 to 20 nm and below over that temperature excursion. Alternatively one could simply spray a very dilute salt solution in the one-phase (vapor) regime. These salt particles could be injected directly into experimental cloud chambers, and the method might be extended to other salts with similar precipitation characteristics or to different solvents.

For deployment in MCB applications requiring 10^{17} CCN per source it is found that the method is overly energy intensive, even if a good fraction of the energy could be retrieved from the waste heat of a vessel. At the outset of this investigation, a 40-nm diameter salt particle was still considered a minimum-sized, but viable CCN. Subsequent theoretical investigations (Latham et al., 2012a) have moved this target closer to 100 nm, in essence increasing the volume that needs to be sprayed by a factor of 15.6. As the resulting particle distribution is not monodisperse, but has a distribution with a GSD close to 2, this imposes another penalty of approximately ten on the required spray volume. Hence the energy cost of a method that in essence evaporates all the water rises dramatically and the technique becomes significantly less attractive.

For a prototype demonstration these dry salt particles do, however, have significant advantages over wet droplets. As the crystals are fully formed when they exit the nozzle, they don't depend on external ambient conditions for evaporation. Ambient air cooling caused by the intense spray may cause liquid-sprayed droplets to reside near the ocean surface for a long time, possibly greatly diminishing their numbers over time. In contrast to wet droplets, under laboratory conditions dry particles are seen to rise and diffuse rapidly, and pass through HEPA filters with astonishing ease. Thus their effectiveness might be substantially better than that of wet droplets. For this reason, even the production of 10^{16} nuclei/s by this method may be suitable for prototype research, particularly if the distribution can be improved to reduce the energy requirements by a factor of five as outlined above.

As compared to air-assisted Taylor cone droplet spraying (Cooper et al., 2013), where the required energy may be as low as 0.4 MW for 10^{17}/s nuclei, the present method requires significantly more energy, while droplets from the former are only partially evaporated by the energy supplied. Distributions with d_g ranging from 60 to 85 nm were made by the Taylor cone method, with GSDs typically of 1.57, and occasionally as low as 1.19. Control of the very large space charge generated by these highly charged particles (including their image charge in the ocean) may prove to be quite challenging at sea, especially if considerable wind is present. We are therefore still considering the exploration of super-effervescent nozzles at very high pressures (>10 kbar) where the presence of two (or more) separate fluids produces small droplets in a range estimated to be suitable for the intended purpose. There is no heating involved and thus the resulting droplets are liquid. In seaborne applications, their drying and lifting may be facilitated by injection into the ship exhaust, after interfering contaminants have been removed from it if necessary, by precipitation.

Acknowledgments

The authors acknowledge the financial support of FICER for part of this work and in particular thank David Keith and Ken Caldera for their encouragement. We thank J. Bischoff and B. Thomas from the USGS for very informative discussions on supercritical seawater, and Qin Wang and David Johnston of Aqua Metrology Systems for their expert help and suggestions with some of the experimental setup. We acknowledge our debt to several suppliers who provided us with free samples, services or expertise: Alex Laymon from DPSS Lasers, Inc. for laser drilling, Bill Peifer from sp3 Diamond Technologies, Inc. for diamond sheets, Alex Shimkunas and Phil Mauger from Nanostructures, Inc., Chris Horton from Cree, Inc., Rich Olazaba from Cal-Weld Inc., Dwight Tanaka from Current EDM, Inc., and Walter Bachman from Bachman Instruments. Part of this work was performed at the Stanford Nanofabrication Facility, supported by the National Science Foundation grant no. ECS-9731293.

Appendix A. Supplementary data

Supplementary data to this article can be found online at http://dx.doi.org/10.1016/j.atmosres.2013.10.025.

References

Abraham, J.P., 2009. Purdue University, private communication.

Albrecht, B., 1989. Aerosols, cloud microphysics, and fractional cloudiness. Science 245, 1227–1230. http://dx.doi.org/10.1126/science.245.4923.1227.

Bala, G., Caldreia, K., Nemani, R., Cao, L., Ban-Weiss, G., Shin, H.-J., 2010. Albedo enhancement of marine cloud to counteract global warming: impacts on the hydrological cycle. Clim. Dyn. 37, 915–931. http://dx.doi.org/10.1007/s00382-010-0868-1.

Bischoff, J.L., 1991. Densities of liquids and vapors in boiling NaCl solution. A PVTX summary from 300° to 500 °C. Am. J. Sci. 291, 307–338. http://dx.doi.org/10.2475/ajs.291.4.309.

Bischoff, J.L., Pitzer, K.S., 1989. Liquid–vapor relations for the system NaCl–H_2O: summary of the P-T-x surface from 300° to 500 °C. Am. J. Sci. 289, 217–249. http://dx.doi.org/10.2475/ajs.289.3.217.

Bischoff, J.L., Rosenbauer, R.J., 1983. A note on the chemistry of seawater in the range 350°–500 °C. Geochim. Cosmochim. Acta 47, 139–144. http://dx.doi.org/10.1016/0016-7037(83)90098-4.

Bischoff, J.L., Rosenbauer, R.J., 1985. An empirical equation of state for hydrothermal seawater (3.2 percent NaCl). Am. J. Sci. 285, 725–763. http://dx.doi.org/10.2475/ajs.285.8.72.

Bower, K., Choularton, T., Latham, J., Sahraei, J., Salter, S., 2006. Computational assessment of a proposed technique for global warming mitigation via albedo enhancement of marine stratocumulus clouds. Atmos. Res. 82, 328–336. http://dx.doi.org/10.1016/j.atmosres.2005.11.013.

Cooper, G., Johnston, D., Foster, J., Galbraith, L., Neukermans, A., Ormond, R., Rush, J., Wang, Q., 2013. A review of some experimental spray methods for marine cloud brightening. Int. J. Geosci. 4, 78–97. http://dx.doi.org/10.4236/ijg.2013.41009.

Crutzen, P.J., 2006. Albedo enhancement by stratospheric sulfur injections: a contribution to resolve a policy dilemma. Clim. Chang. 77 (3–4), 211–219 (doi.org/10.1007%2Fs10584-006-9101-y).

Hatch, T., Choate, S., 1929. Statistical description of the size properties of nonuniform particulate substances. J. Franklin Inst. 207, 369–387. http://dx.doi.org/10.1016/S0016-0032(29)91451-4.

Hudson, J.G., 2009. Division of Atmospheric Sciences, Desert Research Institute, Nevada, Private communication.

Jones, A., Hayward, J., Boucher, O., 2009. Climate impacts of geoengineering marine stratocumulus clouds. J. Geophys. Res. 114, D10106. http://dx.doi.org/10.1029/2008JD011450.

Jones, A., Hayward, J., Boucher, O., 2011. A comparison of the climate impacts of geoengineering by stratospheric SO_2 injection and by brightening of marine stratocumulus clouds. Atmos. Sci. Lett. 12, 176–183. http://dx.doi.org/10.1002/asl.291.

Korhonen, H., Carslaw, K.S., Romakkaniemi, S., 2010. Enhancement of marine cloud albedo via controlled sea spray injections: a global model study of the influence of emission rates, microphysics and transport. Atmos. Chem. Phys. Discuss. 10, 735–761. http://dx.doi.org/10.5194/acpd-10-735-2010.

Latham, J., 1990. Control of global warming? Nature 347, 339–340. http://dx.doi.org/10.1038/347339b0.

Latham, J., 2002. Amelioration of global warming by controlled enhancement of the albedo and longevity of low-level maritime clouds. Atmos. Sci. Lett. 3, 52–58. http://dx.doi.org/10.1006/asle.2002.0099.

Latham, J., Rasch, P., Chen, C.-C., Kettles, L., Gadian, A., Gettelman, A., Morrison, H., Bower, K., Choularton, T., 2008. Global temperature stabilization via controlled albedo enhancement of low-level maritime clouds. Phil. Trans. R. Soc. A 366, 3969–3987. http://dx.doi.org/10.1098/rsta.2008.0137.

Latham, J., Bower, K., Choularton, T., Coe, H., Connolly, P., Cooper, G., Craft, T., Foster, J., Gadian, A., Galbraith, L., Iacovides, H., Johnston, D., Launder, B., Leslie, B., Meyer, J., Neukermans, A., Ormond, B., Parkes, B., Rasch, P., Rush, J., Salter, S., Stevenson, T., Wang, H., Wang, Q., Wood, R., 2012a. Marine cloud brightening. Phil. Trans. R. Soc. A 370, 4217–4262. http://dx.doi.org/10.1098/rsta.2012.0086.

Latham, J., Parkes, B., Gadian, A., Salter, S., 2012b. Weakening of hurricanes via marine cloud brightening (MCB). Atmos. Sci. Lett. 13, 237. http://dx.doi.org/10.1002/asl.402.

Lemmon E.W., McLinden M.O. and Friend D.G., “Thermophysical Properties of Fluid Systems” in NIST Chemistry WebBook, NIST Standard Reference Database Number 69, Eds. P.J. Linstrom and W.G. Mallard, National Institute of Standards and Technology, Gaithersburg MD, 20899, http://webbook.nist.gov, (retrieved February 26, 2013).

Neukermans, A., 1973. Optical sizing of monodisperse toner. Xerox Corporation Technical Report #22302.

Perry, R.H., Green, D.W., 1984. Perry's Chemical Engineers' Handbook, Sixth edition. McGraw–Hill.

Rasch, P., Latham, J., Chen, C.-C., 2009. Geoengineering by cloud seeding: influence on sea ice and climate system. Environ. Res. Lett. 4, 045112. http://dx.doi.org/10.1088/1748-9326/4/4/045112.

Rayleigh, L., 1878. On the instability of jets. Proc. Lond. Math. Soc. 10, 4–13. http://dx.doi.org/10.1112/plms/s1-10.1.4.

Salter, S., Sortino, G., Latham, J., 2008. Sea-going hardware for the cloud albedo method of reversing global warming. Phil. Trans. R. Soc. A 366, 3989–4006. http://dx.doi.org/10.1098/rsta.2008.0136.

Twomey, S., 1977. Influence of pollution on the short-wave albedo of clouds. J. Atmos. Sci. 34, 1149–1152. http://dx.doi.org/10.1175/1520-0469(1977)034<1149:TIOPOT>2.0.CO;2.